



Understanding long-term variations in GPS differential code biases

Yan Xiang¹ · Zhexin Xu² · Yang Gao³ · Wenxian Yu¹

Received: 22 September 2019 / Accepted: 8 September 2020 / Published online: 29 September 2020
© Springer-Verlag GmbH Germany, part of Springer Nature 2020

Abstract

Precise estimation of satellite differential code biases (DCBs) plays a crucial role in precise ionospheric modeling, positioning, and timing. Due to the rank deficiency, a constraint or a datum is required in order to separate the satellite DCBs from the receiver DCBs. A common practice is to impose a zero-mean constraint on all the visible satellites. However, datum selection is affected by satellite replacement and variation of the DCBs. As a result, the long-term variations of current DCB products vary significantly. Taking the DCBs of SVN 44 (PRN 28) as a reference, we analyzed the long-term variations of DCBs over a period of 20 years, between 2000 and 2019. Based on this reference, the results indicate that the change of the zero-mean datum is responsible for the variation of current DCB products. The datum change is attributed to the satellite replacement as well as the discontinuities and their variations. We found that discontinuities for the same satellite vehicle reach 1.8 ns, which is related to satellite changes announced in the Notice Advisory to Navstar Users message and to flex power. The magnitude of the DCBs depends on the satellite type. DCBs for Block IIR-A and IIR-M satellites are close to each other, while DCBs of Block IIR-B satellites are approximately 5 ns larger and DCBs for the Block IIF are 8 ns smaller. In addition, the satellite biases between GPS *P1* and *C1* are also briefly examined, and the results show that they are also affected by the satellite replacements and discontinuities. However, the satellite bias differences between *P1* and *C1* for different satellite types are minor.

Keywords Satellite biases · Differential code biases (DCBs) · Bias discontinuity · Bias jump · Bias variations · Flex power · NANU

Introduction

Global navigation satellite system (GNSS) pseudorange measurements are influenced by different hardware-introduced group delays at different signals. The delays are also known as differential code biases (DCBs) at different frequencies, such as *P1* and *P2*, or at the same frequency for different signals, such as *P1* and *C1* (Gao et al. 2001; Li et al. 2012; Villiger et al. 2019). These hardware delays are caused by the digital signal processing components, antenna, cables, and front-end when signals at both the satellite and

receiver are encoded (Hegarty et al. 2005; Hauschild and Montenbruck 2016). They are nonnegligible error sources in obtaining the absolute ionosphere delays or achieving high precision timing and positioning since the DCBs can be significant, ranging from -10 to 10 ns (Ray and Senior 2005; Levine 2008; Rovira-Garcia et al. 2015; Xiang 2018; Tu et al. 2019).

Previous research has applied the geometry-free combination to estimate the DCBs at different frequencies using ionospheric modeling (Mannucci et al. 1998; Yuan and Ou 2004; Hernández-Pajares et al. 2009; Zhong et al. 2016b). The geometry-free combination cancels the geometry-related components, and the remaining are the frequency-dependent ionospheric delays and biases at the transmitting and receiving side. Due to the noisy pseudorange measurements, the geometry-free combination of the pseudorange measurements is usually smoothed or leveled by the carrier phase measurements. However, this method suffers from leveling or smoothing errors. Further improvement can be made to reduce the leveling errors using the ionospheric

✉ Yan Xiang
yan.xiang@sjtu.edu.cn

✉ Zhexin Xu
xuzhexin@fjnu.edu.cn

¹ Shanghai Jiao Tong University, 800 Dongchuan Road, Shanghai, China

² Fujian Normal University, Fuzhou, China

³ University of Calgary, Calgary, Canada

observables based on precise point positioning (Banville et al. 2012; Zhang et al. 2012; Xiang and Gao 2017).

GNSS scholars have extensively studied DCB estimation (Li et al. 2016, 2017; Montenbruck et al. 2014; Wang et al. 2016; Zhao et al. 2017). Dating back three decades, Coco et al. (1991) and Sardón and Zarraoa (1997) demonstrated the interday stability in terms of root-mean-square, using the limited volume of data within two years. Zhang et al. (2017) characterized the short-term variation of between-receiver DCBs and the relationship between DCBs and temperature. Recently, Wanninger et al. (2017) modeled the short-term DCBs, or group delay variations, as a function of elevation and azimuth. Zhang et al. (2014) investigated whether DCB variations are affected by ionospheric variation or solar cycles, because DCBs are estimated in ionospheric modeling. They found a downward trend in the estimated DCBs based on the data from 1999 to 2010. Then, Zhong et al. (2016a) clarified that the descending drift is independent of the ionospheric variations by choosing continuous operating satellites as a reference from the year of 2002 to 2014. Instead, the results reveal that the DCB variations are related to the satellite replacement and the zero-mean constraint or datum imposed on these satellites. More recently, Villiger et al. (2019), at the Center for Orbit Determination in Europe (CODE), worked on the observable-specific signal bias concerning the same datum to make the biases easy to understand and efficient to transform in computations.

However, the variations, discontinuities, and characteristics are still not well understood and clearly explained. Fortunately, the international GNSS service (IGS) has provided many datasets of DCB products since 1998. It is a substantial resource when researching the temporal variations of DCBs on a long timescale. In this study, choosing a continuous operating satellite as a reference, we attempt to make use of these data to interpret the long-term stability of DCBs. Understanding the characteristics is beneficial to improve the estimation or prediction of DCBs so that they can be applied to ionospheric modeling, high precision timing, and positioning.

The next section explains the method of analyzing the long-term variation of DCBs and describes the data used in the study. Then, the following section displays and discusses the results, answering some crucial questions about DCBs. Finally, the conclusions are briefly summarized.

Methodology and dataset

Before explaining how the long-term variations using the same datum are analyzed, we need to understand how DCBs are calculated. It is well known that the DCBs between different frequencies are commonly computed using ionospheric modeling. The CODE daily DCB solutions are

calculated as part of the global ionospheric modeling effort. The effects of the leveling errors mentioned in the introduction are not considered in the study, because CODE is applying the smoothed code measurements or ionospheric observables (Dach et al. 2015). Ionospheric modeling can be explained by the following equation:

$$\begin{aligned} \tilde{I} &= I_2 - I_1 + (\text{DCB}^s - \text{DCB}^r) + \varepsilon \\ &= \text{MF} \times K \times \text{VTEC}(\varphi_{\text{IPP}}, \lambda_{\text{IPP}}) + (\text{DCB}^s - \text{DCB}^r) + \varepsilon, \end{aligned} \tag{1}$$

where \tilde{I} is the carrier phase smoothed ionospheric observables; I_1 and I_2 are the pseudorange ionospheric delays on the frequency of $L1$ and $L2$, respectively; MF is the mapping function converting the slant ionospheric total electron contents (TEC) to vertical ones; IPP is the interpolated pierce point when the single-layer model is assumed; $\text{VTEC}(\varphi_{\text{IPP}}, \lambda_{\text{IPP}})$ is the vertical TEC as a function of latitude, φ_{IPP} , and longitude, λ_{IPP} , at IPPs; ε is the noise; DCB^s and DCB^r are the satellite and receiver DCBs, respectively; and $K = \frac{f_1^2 - f_2^2}{f_2^2 f_1^2} \times 40.3 \times 10^{16}$ with two carrier frequencies, f_1 and f_2 . Note that, in the case of CODE, the spherical harmonic function is adopted to model the global ionosphere.

It is worth mentioning that the satellite DCBs and the receiver DCBs are linear dependent. The ionospheric modeling has a rank deficiency of one, because each satellite shares the same receiver DCB. To solve this rank deficiency, it is a common practice to add the zero-mean constraint of all the observed satellites as:

$$S \hat{X}_{\text{DCB}} = \mathbf{0}, \text{ where } \hat{X}_{\text{DCB}} = [\hat{X}_{\text{DCB}^s}, \hat{X}_{\text{DCB}^r}], \quad S = [\mathbf{e}, \mathbf{0}] \tag{2}$$

where S is the constraint vector, and the elements are 1 for satellite DCBs and 0 for receiver DCBs; \mathbf{e} contains the elements of 1 with a size of all the visible satellites; \hat{X}_{DCB} refers to the DCB estimates; \hat{X}_{DCB^s} are the satellite DCBs; and \hat{X}_{DCB^r} are the receiver DCBs.

However, the instability of the zero-mean constraint of all satellites raises an issue. Research concluded that this constraint or the datum changes when the DCBs of some satellites are not stable or old satellites are replaced (Li et al. 2012; Zhong et al. 2016a). Instead, choosing a continuous running satellite as a reference offers a way to investigate the long-term variation of other satellite DCBs, given by:

$$\Delta \hat{X}_{\text{DCB}^s} = \hat{X}_{\text{DCB}^s} - \hat{X}_{\text{DCB}^s_{\text{ref}}}, \tag{3}$$

where $\Delta \hat{X}_{\text{DCB}^s}$ are the DCB value with respect to the reference DCBs. It is important to note that these differences are utilized for analysis in the study.

The DCB products from 2000 to 2019 are analyzed. Furthermore, because of minor differences existing between the CODE and other IGS analysis centers (Wang et al. 2016),

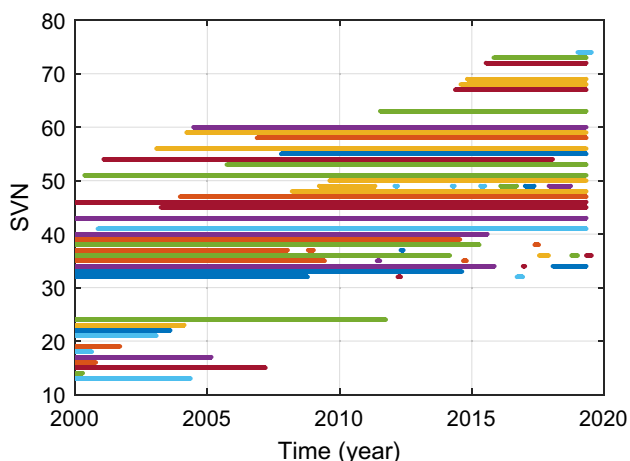


Fig. 1 All GPS satellites launched from 2000 to 2019, identified by the satellite vehicle number (SVN). The horizontal axis indicates the operating time. Each color represents a continuous operating period

we chose the DCB products from CODE in the study. All the satellite vehicles that were launched in the specified time frame are exhibited in Fig. 1. This figure is plotted based on the satellite-specific information available in the file SATTLITE.I14 (<https://ftp.aiub.unibe.ch/BSWUSER52/GEN/SATELLIT.I14>). The horizontal line represents the operating time. The daily and monthly DCB products between $P1$ and $P2$ are accessible at CODE. Both are available on websites (<https://ftp.aiub.unibe.ch/CODE>). It is of interest to note that the daily products are located as part of the global ionospheric maps in the format of IONEX (ionosphere exchange) and are not in a separate daily file similar to the monthly products. Here, the biases of GPS are only examined due to

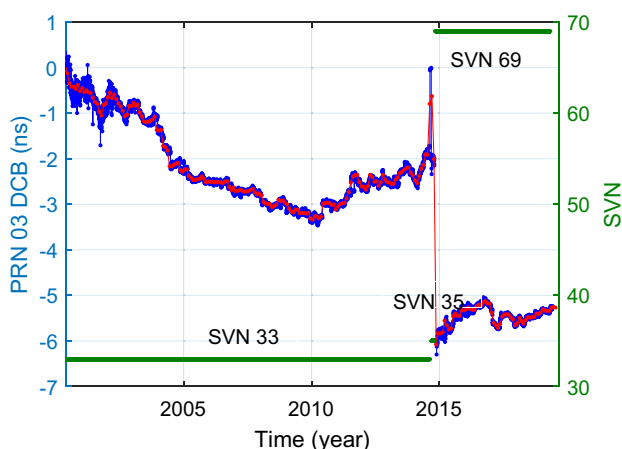


Fig. 2 DCB time series of PRN 03 (SVN 33, SVN 35, SVN 69). On the left y-axis, blue indicates the daily DCBs, and red is monthly DCBs. The green line, which corresponds to the y-axis on the right, indicates SVN. The jump in the green line indicates that the PRN 03 was assigned to another vehicle

its longer operability. DCBs refer to interfrequency DCBs between satellite signals $P1$ and $P2$.

An example of a time series of daily and monthly DCB products for PRN 03 (SVN 33, SVN 35, SVN 69) is displayed in Fig. 2. Blue represents the daily DCBs and red represents the monthly ones. The time scale on the x -axis for the monthly solutions is set to the middle of the month. The right axis indicates the SVN in green. Generally, the daily and monthly data present a fairly consistent trend, and the monthly data are slightly smoother than the daily solutions because of averaging. There is an obvious decreasing trend from the beginning to the year 2010 and an increasing trend afterward until a negative jump occurred around 2015. The variation is related to the variation in the zero-mean datum imposed on all the DCB estimations. The reason why there is a jump to a negative value is that PRN 03 is reassigned from a Block IIA satellite to a Block IIF satellite. This will be further explained in the following subsections.

To ensure a stable and continuous datum, we choose a satellite as a reference that has been continuously operating for a long time. As explained in Villiger et al. (2019), SVN 44, i.e., PRN 28 is stable and has served continuously since its launch. Therefore, PRN 28 is chosen as a reference. The DCB values for PRN 28 are illustrated in Fig. 3. It can be seen that the DCB trendline for PRN 28 is continuous and without prominent discontinuities. The data starting at 2000, rather than 1998, are analyzed, because PRN 28 began operation in August 2000.

By choosing the reference, the relative DCBs of PRN 03 with respect to PRN 28 are presented in Fig. 4. It is apparent that the relative DCBs for PRN 03 are much more stable when comparing to Figs. 2 and 3. A similar trend is removed when the differences are created.

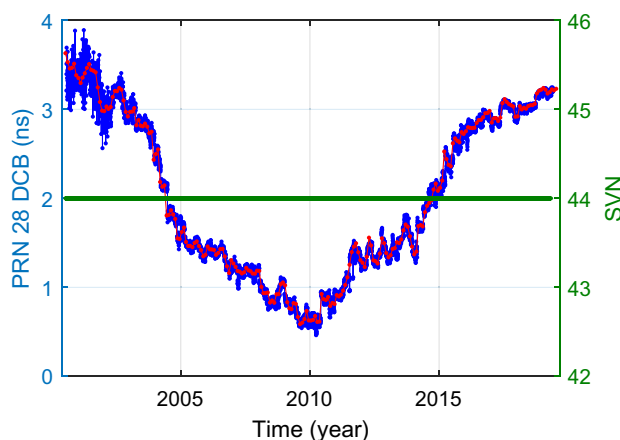


Fig. 3 DCB time series for continuous operating PRN 28 (SVN 44). The green line, corresponding to the right y-axis, refers to SVNs

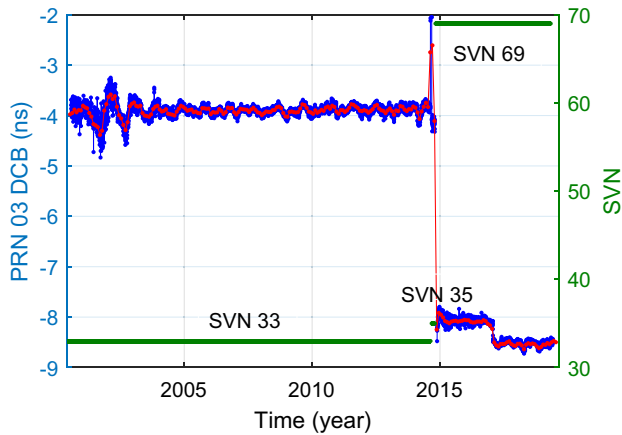


Fig. 4 DCB time series for PRN 03 (SVN 33, SVN 35, SVN69) with reference to PRN 28 (SVN 44). The green line, corresponding to the right y-axis, refers to SVN

Results and discussions

Below, we attempt to answer the following questions: (1) How is the datum related to the variations in current DCB products? (2) What caused the jumps for a continuous operating satellite as a function of satellite status and flex power? (3) Would the DCBs be affected by ionospheric modeling? (4) How are the DCB values related to different PRNs when the same SVN is assigned to different PRNs? (5) What are the characteristics of different types of GPS satellites and how stable are the biases? (6) Do the results of DCBs apply to the biases between P1 and C1?

DCB variations related to the zero-mean datum

Instead of displaying the current DCB products, the DCB variations with respect to the PRN 28 from randomly selected satellites are presented in Fig. 5. The left y-axis is the relative DCBs to PRN 28 and the right y-axis is SVN plotted in green. The figure confirms that the DCBs are stable and that there are jumps when the SVN is changed (green) throughout this 20-year period. If we assume that the DCBs of PRN 28 are stable based on the research of Viliger et al. (2019), the result reveals that the satellite DCBs are stable after differencing with PRN 28, suggesting that their variations are affected by a similar trend. As mentioned in the methodology section, a zero-mean datum is imposed when DCBs are estimated. We believe the datum is one of the contributors to this trend. However, further demonstration is required to determine whether the trend could be caused by temperature or the ionospheric activities.

Further attention must be paid to the usage of the monthly products. As previously explained, the monthly data trend is smoother than the daily data trend because of the averaging. However, the monthly data need to be used with caution during satellite replacement. This is because the monthly data could be the average of two different DCBs from two SVNs. For example, the monthly data of PRN 09 in the middle are deteriorated during the time of satellite replacement.

In general, the satellite DCBs are stable for the same SVN. However, some discontinuities are noticeable, even for the same SVN, which is caused by the satellite status changes. An example is PRN 02 around 2014. Some satellites are stable, such as PRN 05 and PRN 06, but some descend in the long-term, such as PRN 13. These variations

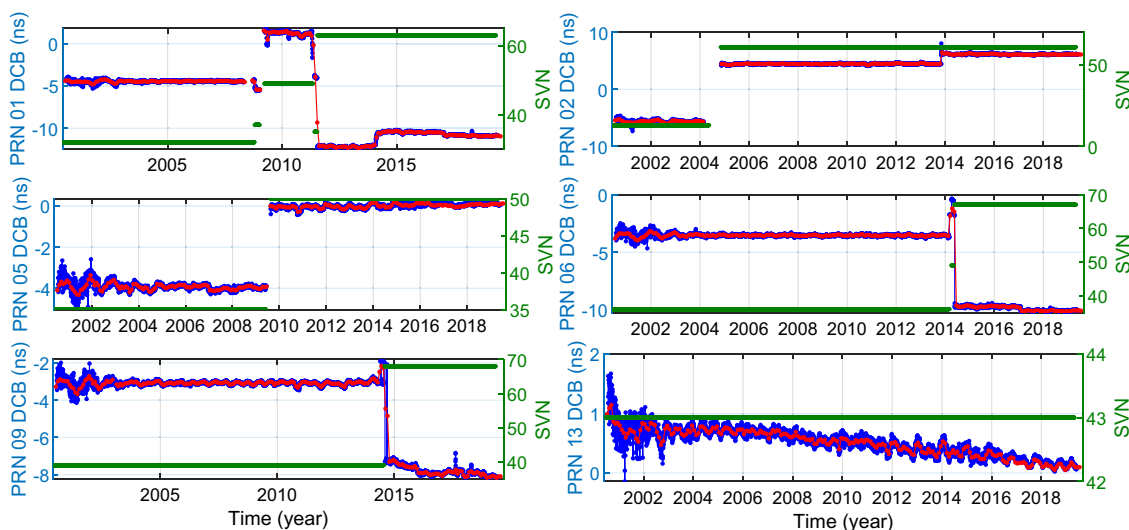


Fig. 5 Time series of selected satellite DCBs (PRNs) referenced to PRN 28 in units of nanoseconds. The green line, corresponding to the right y-axis, refers to SVN

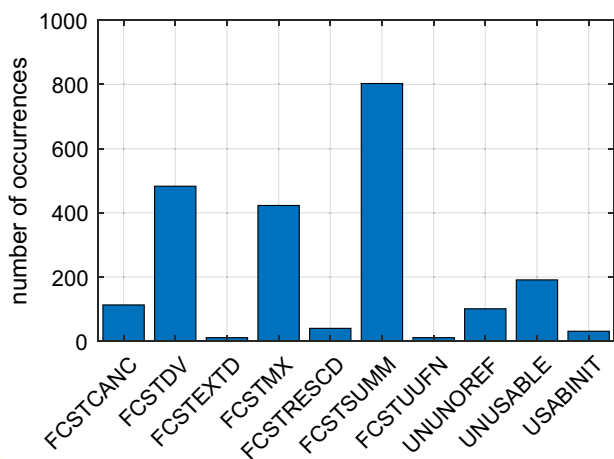


Fig. 6 Statistics on the occurrence of NANU events. NANU events starting with “FCST” are the scheduled events; others are not. There is a total of 10 NANU message types

for the same SVN will be explained in the following subsections.

DCB discontinuities related to satellite status

Previous subsections indicate that the DCBs of the same satellite vehicle usually remain stable, but discontinuities for the same satellite vehicle, such as PRN 02 (SVN61) in Fig. 5, are also observed. Villiger et al. (2019) mentioned that some of the discontinuities are related to Notice Advisory to Navstar Users (NANU) messages, which describe the satellite changes in the constellations. These changes are maneuvers or onboard equipment maintenance. The information on the NANU can be found on their website (<https://www.navcen.uscg.gov/?pageName=nanu>). Figure 6 summarizes the statistics of ten types of scheduled and unscheduled NANU events with a total of 2378 events. NANU events starting with “FCST” are the scheduled events, and the remainder are the unscheduled events. The reason why the occurrence of “FCSTSUMM” is higher than other events is that it is the summary of all the scheduled events. Further details on what each type means are given at <https://www.navcen.uscg.gov/?pageName=nanuAbbreviations>.

A selection of discontinuity examples for the same satellite vehicle per panel is exhibited in Fig. 7. It can be noticed that SVN 25 dropped obviously around the year 2006 and recovered to the previous value. This drop is related to NANU event numbers 2005159 (UNUSABLE) and 2006058 (UNUSABLE). SVN 47 presented two discontinuities: NANU 2008078 (FCSTMX) on the forecast outage and NANU 2010134 (FCSTSUMM) on the summary of unusable status until further notice. Additionally, SVN 47 starts

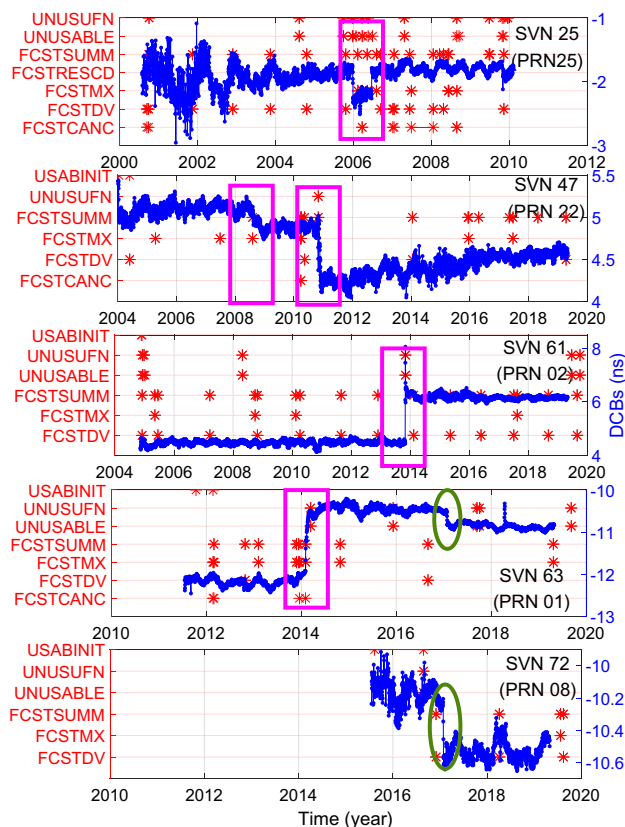


Fig. 7 DCB discontinuities (dark blue) for the same satellite vehicle per panel and NANU events (red star). The DCB discontinuities in the rectangles are related to NANU messages. The green ellipses highlight the shifts due to flex power

to increase from late 2010, which matches the trend given in Villiger et al. (2019). For SVN 61, the discontinuity is up to approximately 1.8 ns and maintains this value afterward. This is related to NANU 2013062 (UNUSABLE). For SVN 63, a discontinuity in the green circle around 2017 is noticed, but no specific NANU event was found. The nearest one is still far from this point. A similar case is observed with SVN 72. Actually, these discontinuities are related to the flex power, which will be explained in the next subsection.

Therefore, we believe that some of the discontinuities are related to the occurrence of NANU messages, but NANU messages do not necessarily causes discontinuities. In fact, Fig. 7 indicates that the occurrence rate of NANU events relating to DCB discontinuities is low, because only a few NANU events result in the DCB discontinuities. Furthermore, the challenge to building the connection between NANU events and the discontinuities is determining how to define a jump or discontinuity. This is because some day-to-day variations are changing gradually rather than showing an apparent jump, such as SVN 47 around 2008. Additionally, some overlap between the NANU events and other events could last for several days.

DCB shift related to flex power

GPS satellites usually transmit their signals at constant power. Flex power redistributes the power between different signals to protect users from jamming. The Block IIR-M and IIF types of satellites are capable of performing flex power. Recently, Steigenberger et al. (2019) explained three types of flex power modes. In the first type of flex power, 10 out of 12 Block IIF satellites have utilized flex power since January 27, 2017. The second type is a four-day flex power usage from April 13 to 17, 2018. The third type is an 11-h flex power usage for three days on April 27, May 1 and 4, 2018.

A selection of shifts due to the flex power for Block IIF satellites is presented in Fig. 8. The red line indicates January 27, 2017, which is the time of the first type of flex power. An obvious shift can be observed before and after this time. The shift is up to 0.4 ns. The green ellipses emphasize the spike around April 15, 2018 at the second type of flex power. The spike is up to 0.5 ns. The third type of 11-h flex power did not have an apparent shift for these satellites. However, tiny bumps of approximately 0.2 ns were noticed for SVN73 for the 11-h flex power, as shown in red in Fig. 9.

DCBs related to solar activities

As explained in the methodology section, the satellite DCBs are estimated together with ionospheric modeling. It is of interest to know how the DCB variations are related to solar activities, since the latter directly affects the ionospheric

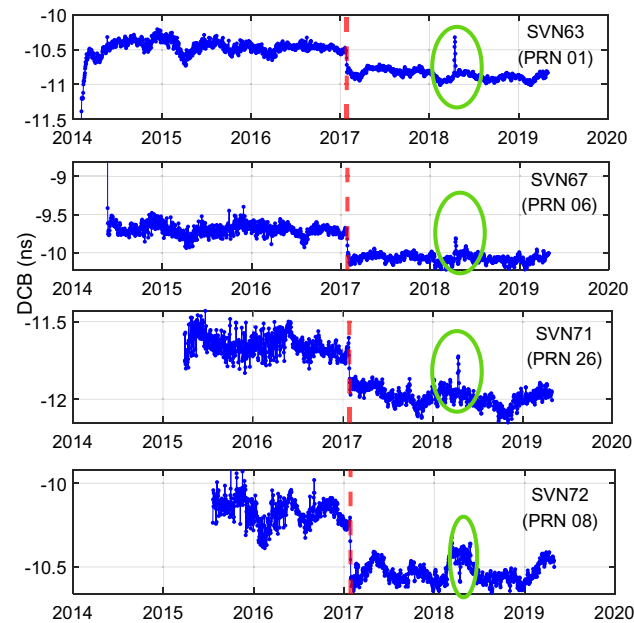


Fig. 8 DCB shifts due to flex power. The red dashed line identifies January 27, 2017. The green ellipses are located around April 15, 2018

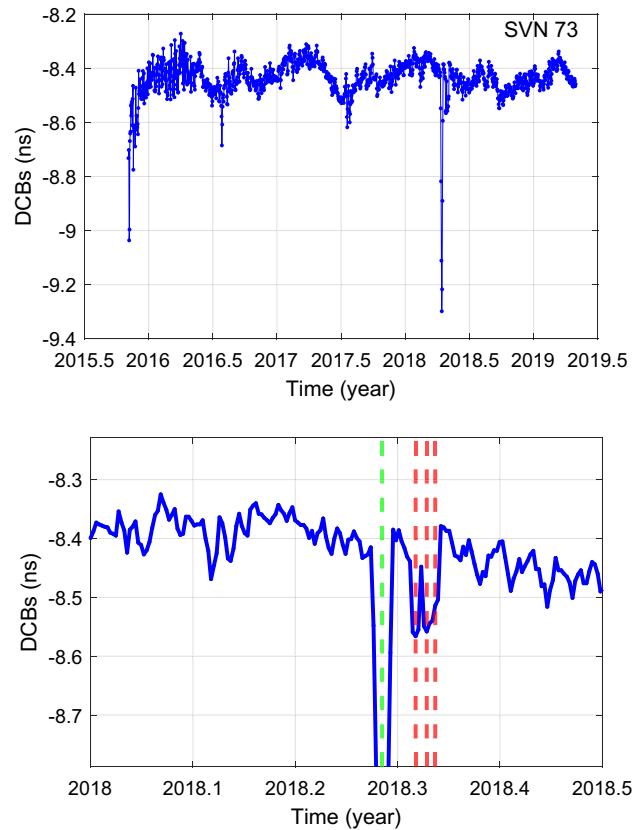


Fig. 9 DCB shift due to flex power for SVN 73 (PRN 10). The bottom figure is a magnified time window. The dashed green and red lines indicate April 15, April 27, May 1 and 4, 2018, respectively

variations. From Figs. 4 and 5, the variations have a close relationship with the zero-mean datum. Here, the relationship between the stability of satellite DCBs the solar activities is explored.

Figure 10 indicates the monthly average f10.7 flux and the single differences in DCBs between two consecutive days. The f10.7 index measures the noise level at a wavelength of 10.7 cm at the earth’s orbit generated by the sun. The larger f10.7 values indicate higher levels of solar activity. A cursory check of the figure shows two noisy places around 2001 and 2015. These two years are high solar activity years in accordance with the f10.7 flux, and the f10.7 flux in 2015 is smaller than that in 2001. The noise level of selected DCBs around 2015 is less substantial than that in 2001. These effects on the noise level of DCBs may be related to the ionospheric modeling or temperature variations (Coster et al. 2013) caused by solar cycles. Due to the lack of temperature information, we cannot confirm the reason of large noise level for the current data analysis.

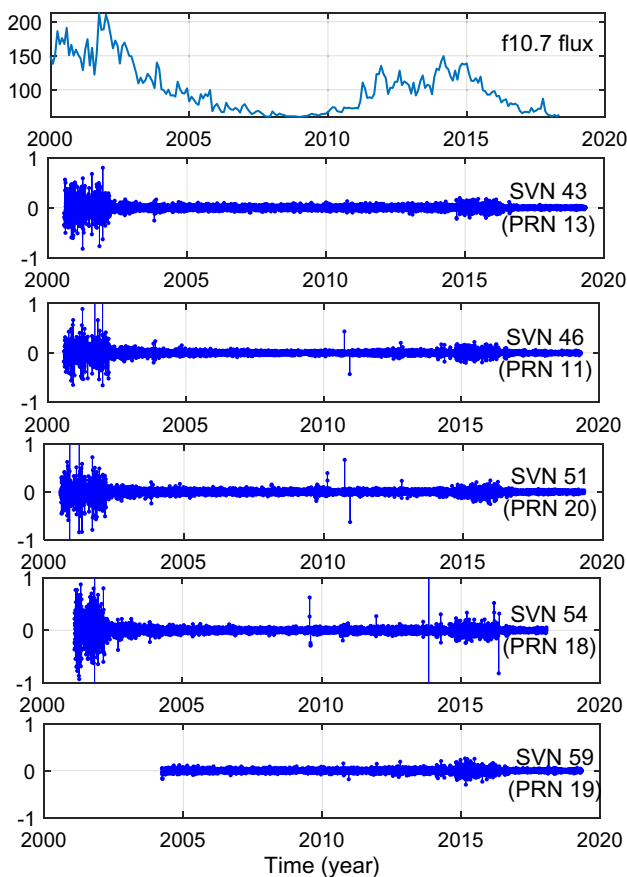


Fig. 10 Monthly average f10.7 flux (top panel) and single difference of daily DCBs between two consecutive days for selected satellites

DCBs related to SVNs

Would the same SVN have the same DCB value if assigned different PRNs? Referring to Fig. 1, one can see that most SVNs have the same respective PRN throughout their lifetime, which is represented using a continuous line. However, some SVNs such as SVN 32, 34, 35, 36, 37, and 49 are assigned different PRNs throughout their lifetime, which is represented by line segments. The DCBs for these six satellites are given in Fig. 11 to show what their DCBs look like.

It is interesting to observe that most DCBs keep similar values, even for different PRNs, but jumps do occur, such as for PRN 49. There are also some spikes of DCBs at each end of the assignment for PRN 49. These spikes are abnormal, caused by averaging and changes of satellite status. Figure 11 also shows that the datum of all visible satellites is affected by the new SVNs that were assigned in partway. Similarly, monthly solutions can be affected by the average of daily solutions. Generally, the results reveal that the DCBs are directly related to SVNs and unrelated to PRNs.

DCBs relate to satellite types

It is well known that the GPS constellation is being modernized. There are 31 satellites in service, and four types of satellites in use: 7 Block IIR-A, 4 Block IIR-B, 7 Block IIR-M, and 12 Block IIF satellites. Further detail on the types of satellite is summarized in the file SATELLITE.I14. The DCBs, separated by satellite type, are presented in Fig. 12 to examine the characteristics of DCBs based on different types of satellites. The time scale on the x-axis infers that the Block IIR-A satellites were launched first, and the Block IIF satellites were the most recently launched ones.

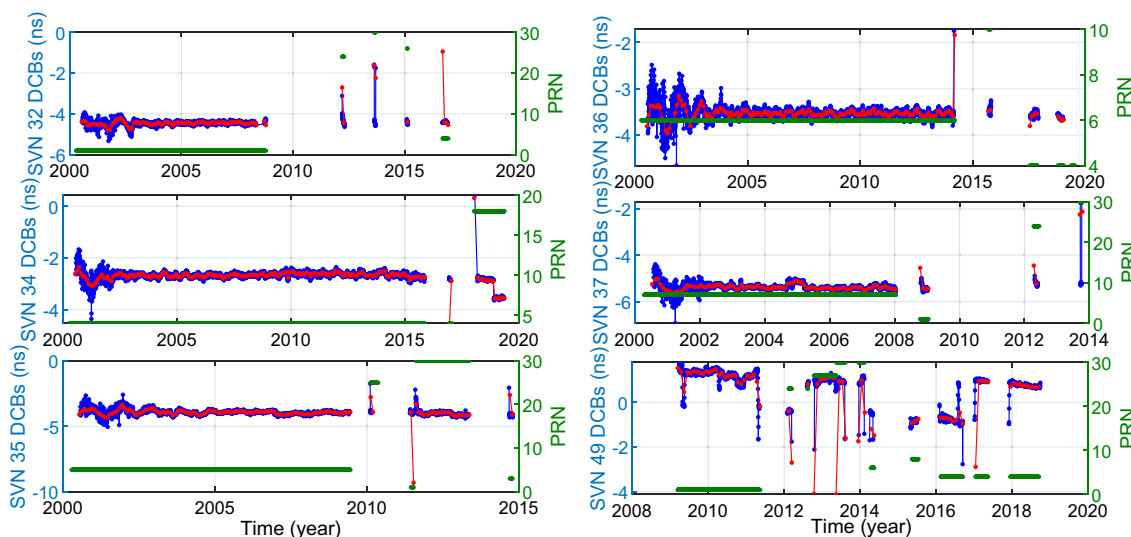


Fig. 11 SVNs with changed PRN assignment. The left axes refer to DCBs in units of ns. The right axis identifies the PRN, here plotted in green

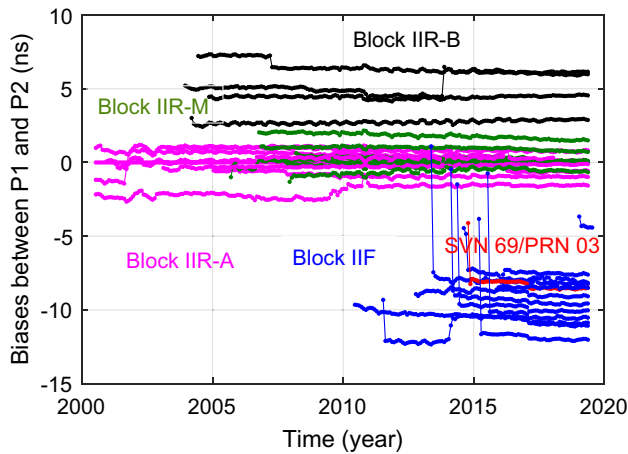


Fig. 12 Monthly DCBs between *P1* and *P2* for each operating satellite vehicle. Different colors represent different satellite types. Here, SVN 69/PRN 03 is highlighted as a Block IIF satellite

It is worth keeping in mind that PRN 28, a Block IIR-A satellite, is chosen as a reference. It can be observed that the DCBs for Block IIR-A satellites in magenta are basically within 1 ns of each other, except for one at the bottom that is approximately 2 ns away. The DCBs in black are for Block IIR-B satellites, and their values are approximately 5 ns larger than those of Block IIR-A satellites. Comparably, the DCBs of Block IIR-M satellites in green are close to those of the Block IIR-A satellites as well, with a difference of approximately 1 ns. By contrast, satellites of Block IIF are approximately 8 to 12 ns smaller compared to those of Block IIR-A.

Therefore, it is not difficult to understand the variations in original DCB products for PRN 03. If the zero-mean

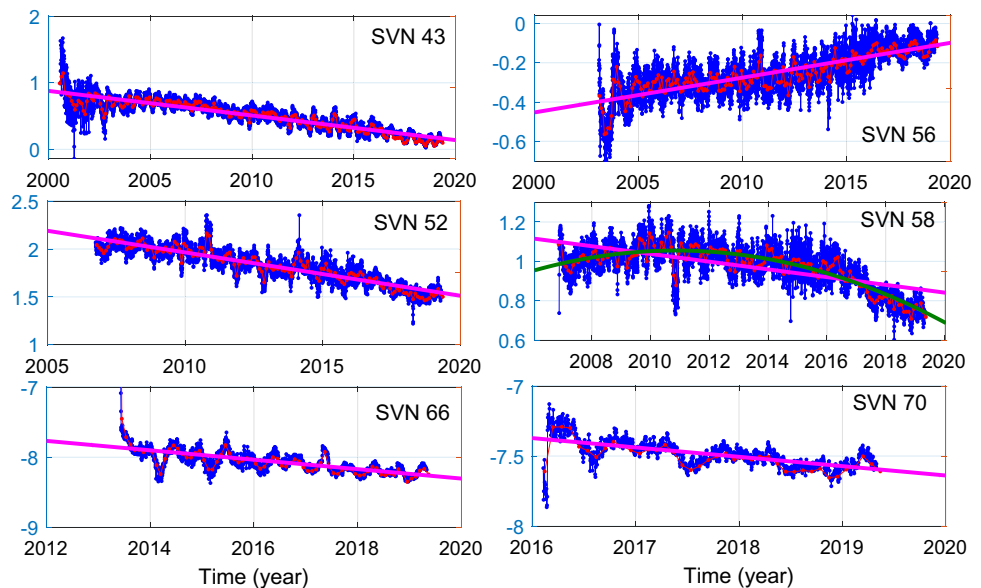
datum of all the DCBs increases, each DCB will decrease to compensate for the zero-mean constraint, and vice versa. For the original DCBs of PRN 03 in Fig. 2, there is a descending trend until 2010, because the datum increases with the launch of Block IIR-B satellites around 2005. The increasing trend around 2010 is caused by the decreasing datum with the launch of the first Block IIF satellites, Block IIF having a smaller DCB. The reason for the negative jump around 2015 is that the PRN 03 was assigned to a Block IIF satellite.

One can observe from the previous figures that some DCBs show slight variations, even without the satellite replacement or the discontinuities. By choosing six continuously operating satellite vehicles from different satellite types, we modeled the daily DCB linearly or quadratically, as demonstrated in Fig. 13. The magenta line and green curve describe the linear and quadratic fittings, respectively. The scale factors or slope for the Block IIR-A satellites SVN 43 and 56 are 0.037 and 0.018, respectively, whereas the scale for the Block IIF satellites SVN 67 and SVN 70 is up to 0.067. Additionally, SVN 58 of Block IIR-M presents a quadratic trend. This linear or quadratic fitting can be employed for the prediction. It is based on different satellite DCB characteristics. Finally, the peak-to-peak amplitude of DCB variations is approximately 0.3 ns (9 cm). If one centimeter (0.03 ns) accuracy of DCB corrections is required for high precision ionospheric modeling, positioning, or timing, the stochastic element must be handled properly.

Biases between *P1* and *C1*

Based on a similar strategy, the biases between *P1* and *C1* are also examined to analyze whether they are affected by

Fig. 13 Linear and quadratic fitting of continuous DCBs. The line and curve describe the linear and quadratic fits



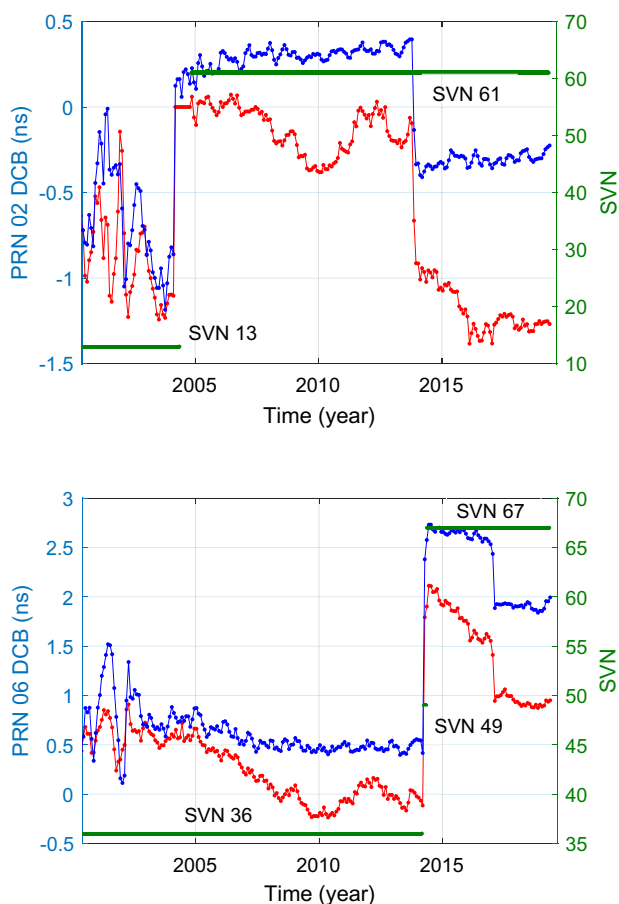


Fig. 14 Monthly biases between $P1$ and $C1$ for PRN 02 (SVN 13, SVN 61) and PRN 06 (SVN 36, SVN 49, SVN 67). On the left axis, blue represents PRN 28 and red represents the original product of biases between $P1$ and $C1$. The axis on the right is the PRN plotted in green

the satellite replacement and discontinuity related to NANU. Figure 14 displays the selection of satellites PRN 02 and PRN 06. In this figure, blue represents PRN 28, and red represents the original bias products between $P1$ and $C1$. One can discern that the relative value in blue is more stable than the original monthly biases between $P1$ and $C1$. Biases between $P1$ and $C1$ are also related to the satellite replacement. For example, PRN 02 and PRN 04 both have a jump during satellite replacement. Additionally, the discontinuity for biases between $P1$ and $C1$ is related to NANU messages. For instance, a discontinuity for PRN 02 around 2014 is similar to the biases between $P1$ and $P2$ mentioned earlier.

Monthly biases between $P1$ and $C1$ for each satellite vehicle are presented in Fig. 15 to show a general picture of bias between $P1$ and $C1$. Overall, biases for $P1$ and $C1$ are within 2 ns, and they are mostly smaller than the biases between $P1$ and $P2$. In addition, unlike the biases between $P1$ and $P2$

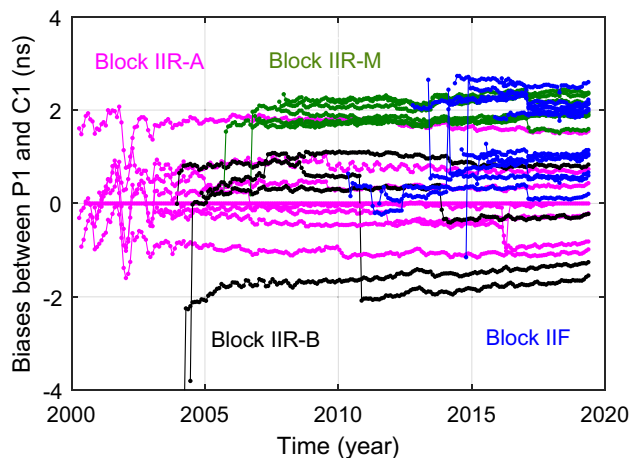


Fig. 15 Monthly biases between $P1$ and $C1$ for each operating satellite vehicle. Different colors represent different satellite types

reflecting the satellite types, biases between $P1$ and $C1$ for different satellite types do not show apparent differences.

Conclusions

By choosing a stable and continuous satellite as a reference, we have studied the long-term variations in GPS satellite biases between $P1$ and $P2$ as well as between $P1$ and $C1$ using CODE products from 2000 to 2019. The method of constraining all the visible satellites to a zero-mean reference makes the long-term DCBs challenging to interpret. Instead, this study chose to select the continuously operating satellite vehicle SVN 44 (PRN 28) as the reference to analyze the long-term variation in DCBs. The results show that the selection of stable and robust references makes a significant difference in understanding the long-term analysis.

In summary, the six factors of zero-mean datum, satellite status, flex power, solar activities, PRNs, and satellite types are considered. The major conclusions can be drawn as follows:

1. The change in the zero-mean datum causes the long-term variations in DCBs. The datum change is attributed to the replacement of satellites as well as the discontinuities and variations of the DCBs.
2. It is necessary to apply the DCB products with caution. This is because the monthly DCBs could be the average of DCBs from two different satellite vehicles.
3. Discontinuities due to NANU message are identified for the same satellite vehicle, and they can be up to 1.8 ns. However, NANU occurrences do not necessarily result in discontinuities. The rate of NANU events occurring and relating to DCB discontinuities is low.

4. Flex power also causes the DCB shift, and this shift is up to 0.4 ns.
5. The DCB estimates under high solar activity conditions are noisier when compared to the low solar activity year.
6. A satellite with different PRNs assigned shows a similar level of DCBs. This concludes that DCBs are highly dependent on satellite vehicles.
7. Different satellite types manifest different amplitudes of DCBs. DCBs for Block IIR-A and IIR-M are close to each other, while DCBs for Block IIR-B is approximately 5 ns larger than that of Block IIR-A. Block IIF is 8–12 ns smaller than that of Block IIR-A. Additionally, the DCBs signify slightly linear or quadratic variations. The peak-to-peak amplitude for this variation is approximately 0.3 ns.
8. Satellite biases between $P1$ and $C1$ are also affected by the satellite replacement and discontinuities related NANU messages, but there are minor differences for different satellite types.

By analyzing the long-term variations of DCBs over a 20-year period, the results indicate that the DCBs are affected by satellite replacement and status changes. The long-term variation in DCBs is caused by the zero-mean datum that is imposed during estimation. In this way, DCBs may potentially act as an indicator of satellite status, alerting users to apply DCBs with caution. In addition, the study assumes that the DCBs of satellites with PRN 28 are continuous and stable. However, these DCBs are also affected by noises, temperature, and NANU events. It would be extremely meaningful to maintain a stable datum to calibrate and estimate the biases. Further research can be done to determine DCBs relative to such a stable datum instead of imposing the zero-mean datum.

Acknowledgements DCB products downloaded from CODE and NANU information are gratefully acknowledged. We also thank anonymous reviewers for their useful comments and suggestions on the research that led to this manuscript. Special thanks to IEEE life fellow Trieu-Kien Truong and Daniele Sartori's proofreading. The study is supported by the science and technology project of State Grid Corporation of China (No. SGSHJX00KXJS1901531).

References

- Banville S, Zhang W, Ghoddousi-Fard R, Langley RB (2012) Ionospheric monitoring using "integer-levelled" observations. In: Proceedings of the ION GNSS 2012, Institute of Navigation, Nashville, Tennessee, USA, September 17–21, pp 2692–2701
- Coco DS, Coker C, Dahlke SR, Clynych JR (1991) Variability of GPS satellite differential group delay biases. *IEEE Trans Aerosp Electron Syst* 27(6):931–938. <https://doi.org/10.1109/7.104264>
- Coster A, Williams J, Weatherwax A, Rideout W, Herne D (2013) Accuracy of GPS total electron content: GPS receiver bias temperature dependence. *Radio Sci* 48(2):190–196. <https://doi.org/10.1002/rds.20011>
- Dach R, Hugentobler U, Fridez P, Meindl M (2015) Bernese GPS software version 5.2. Astronomical Institute, University of Bern
- Gao Y, Lahaye F, Hérroux P, Liao X, Beck N, Olynyk M (2001) Modeling and estimation of $C1-P1$ bias in GPS receivers. *J Geod* 74(9):621–626
- Hauschild A, Montenbruck O (2016) A study on the dependency of GNSS pseudorange biases on correlator spacing. *GPS Solut* 20(2):159–171
- Hegarty CJ, Powers ED, Fonville B (2005) Accounting for timing biases between GPS, modernized GPS, and Galileo signals. In: Proceedings of the ION GNSS 2005, Institute of Navigation, Long Beach, CA, US, September 16–19, pp 2401–2407
- Hernández-Pajares M, Juan JM, Sanz J, Orus R, Garcia-Rigo A, Feltens J, Komjathy A, Schaer SC, Krankowski A (2009) The IGS VTEC maps: a reliable source of ionospheric information since 1998. *J Geod* 83(3–4):263–275
- Levine J (2008) A review of time and frequency transfer methods. *Metrologia* 45(6):S162
- Li H, Li B, Lou L, Yang L, Wang J (2016) Impact of GPS differential code bias in dual- and triple-frequency positioning and satellite clock estimation. *GPS Solut*. <https://doi.org/10.1007/s10291-016-0578-1>
- Li M, Yuan Y, Wang N, Li Z, Li Y, Huo X (2017) Estimation and analysis of Galileo differential code biases. *J Geodesy* 91(3):279–293
- Li Z, Yuan Y, Li H, Ou J, Huo X (2012) Two-step method for the determination of the differential code biases of COMPASS satellites. *J Geod* 86(11):1059–1076
- Mannucci AJ, Wilson BD, Yuan DN, Ho CH, Lindqwister UJ, Runge TF (1998) A global mapping technique for GPS-derived ionospheric total electron content measurements. *Radio Sci* 33(3):565–582
- Montenbruck O, Hauschild A, Steigenberger P (2014) Differential code bias estimation using multi-GNSS observations and global ionosphere maps. *Navigation* 61(3):191–201
- Ray J, Senior K (2005) Geodetic techniques for time and frequency comparisons using GPS phase and code measurements. *Metrologia* 42(4):215–232
- Rovira-García A, Juan JM, Sanz J, Gonzalez-Casado G (2015) A worldwide ionospheric model for fast precise point positioning. *IEEE Trans Geosci Remote Sens* 53(8):4596–4604
- Sardón E, Zarraoa N (1997) Estimation of total electron content using GPS data: how stable are the differential satellite and receiver instrumental biases? *Radio Sci* 32(5):1899–1910
- Steigenberger P, Thörlert S, Montenbruck O (2019) Flex power on GPS block IIR-M and IIF. *GPS Solut* 23(1):8
- Tu R, Zhang P, Zhang R, Liu J, Lu X (2019) Modeling and performance analysis of precise time transfer based on BDS triple-frequency un-combined observations. *J Geod* 93(6):837–847
- Villiger A, Schaer S, Dach R, Prange L, Sušnik A, Jäggi A (2019) Determination of GNSS pseudo-absolute code biases and their long-term combination. *J Geod* 93(9):1487–1500. <https://doi.org/10.1007/s00190-019-01262-w>
- Wang N, Yuan Y, Li Z, Montenbruck O, Tan B (2016) Determination of differential code biases with multi-GNSS observations. *J Geod* 90(3):209–228
- Wanninger L, Sumaya H, Beer S (2017) Group delay variations of GPS transmitting and receiving antennas. *J Geod* 91(9):1099–1116
- Xiang Y (2018) Carrier phase-based ionospheric modeling and augmentation in uncombined precise point positioning. Dissertation, University of Calgary, Calgary, Canada
- Xiang Y, Gao Y (2017) Improving DCB estimation using uncombined PPP. *Navigation* 64(4):463–473

- Yuan Y, Ou J (2004) Generalized trigonometric series function model for determining ionospheric delay. *Prog Nat Sci* 14(11):1010–1014
- Zhang B, Teunissen PJG, Yuan Y (2017) On the short-term temporal variations of GNSS receiver differential phase biases. *J Geod* 91(5):563–572
- Zhang BC, Ou JK, Bin YY, Li ZS (2012) Extraction of line-of-sight ionospheric observables from GPS data using precise point positioning. *Sci China Earth Sci* 55(11):1919–1928
- Zhang D, Shi H, Jin Y, Zhang W, Hao Y, Xiao Z (2014) The variation of the estimated GPS instrumental bias and its possible connection with ionospheric variability. *Sci China Technol Sci* 57(1):67–79
- Zhao L, Ye S, Song J (2017) Handling the satellite inter-frequency biases in triple-frequency observations. *Adv Space Res* 59(8):2048–2057. <https://doi.org/10.1016/j.asr.2017.02.002>
- Zhong J, Lei J, Dou X, Yue X (2016a) Is the long-term variation of the estimated GPS differential code biases associated with ionospheric variability? *GPS Solut* 20(3):313–319
- Zhong J, Lei J, Yue X, Dou X (2016b) Determination of differential code bias of GNSS receiver onboard low earth orbit satellite. *IEEE Trans Geosci Remote Sens* 54(8):4896–4905

Publisher's Note Springer Nature remains neutral with regard to jurisdictional claims in published maps and institutional affiliations.



Yan Xiang is an assistant professor at Shanghai Jiao Tong University. She obtained her Ph. D. in the Department of Geomatics Engineering at University of Calgary. Her current research interests include inter-frequency and inter-system code and phase bias determination, carrier-phase-based ionospheric modeling, and ionospheric augmentation for high precision positioning.



Zhixin Xu received his Ph. D. degree from the School of Informatics at Xiamen University in 2012 and is currently an associate professor in the College of Photonic and Electronic Engineering, Fujian Normal University, Fuzhou. His research interests include wireless networking, image processing, and data mining and analytics.



Yang Gao (Ph. D., Geomatics Engineering, University of Calgary) is a Professor in the Department of Geomatics Engineering at the University of Calgary, Canada. His research interests include theoretical aspects and practical applications of satellite positioning and navigation systems. His current research focuses on high-precision GNSS positioning and multi-sensor integrated navigation systems.



Wenxian Yu (Senior Member, IEEE) is currently with the School of Electronic Information and Electrical Engineering, Shanghai Jiao Tong University. He is also a Yangtze River Scholar Distinguished Professor and the Head of Research. His research interests include radar target recognition, remote sensing information processing, multi-sensor data fusion, and integrated navigation.